ACS Catalysis

RESEARCH ARTICLE

pubs.acs.org/acscatalysis

Identification of Sulfur-Tolerant Bimetallic Surfaces Using DFT Parametrized Models and Atomistic Thermodynamics

Nilay İnoğlu[†] and John R. Kitchin*[,†,‡]

[†]Department of Chemical Engineering, Carnegie Mellon University, Pittsburgh Pennsylvania 15213, United States

[‡]National Energy Technology Laboratory, Pittsburgh, Pennsylvania 15236, United States

Supporting Information

ABSTRACT: The identification of sulfur-tolerant alloys for catalytic applications is difficult due to the combinatorially large number of alloy compositions and surface structures that may be considered. Density functional theory calculations (DFT) are not fast enough to enumerate all the possible structures and their sulfur tolerance. In this work, a DFT parametrized algebraic model that accounts for structure and composition was used to estimate the d-band properties and sulfur adsorption energies of 370 transition metal-based bimetallic alloy surfaces. The estimated properties were validated by DFT calculations for 110 of the surface structures. We then utilized an atomistic thermodynamic framework that includes surface segregation, the presence of adsorbates, and effects of environmental conditions to identify alloy compositions and structures with enhanced sulfur tolerance that are likely to be stable under the environmental conditions. As a case study, we show how this database can be used to identify sulfur-tolerant Cu-based catalysts and compare the results with what is known about these catalysts experimentally.

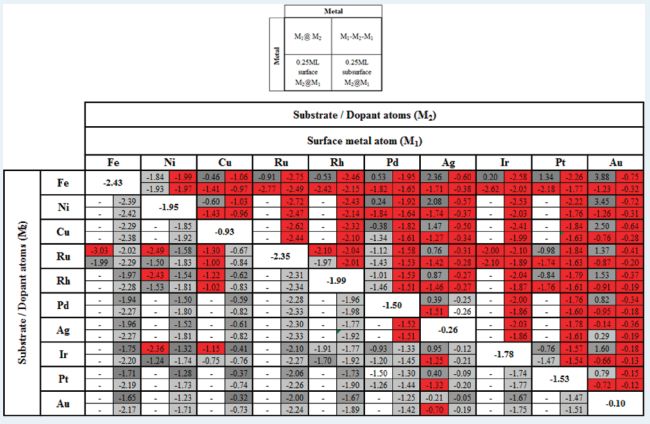

KEYWORDS: sulfur tolerance, bimetallic surface structures, electronic structure modification, d-band width formalism, solid state table, segregation, atomistic thermodynamics

INTRODUCTION

Transition metal catalysts are frequently employed in chemical processes. Sulfur (S)-containing molecules are common impurities in fossil fuel-derived feedstocks and one of the major problems associated with the use of these metal-based catalysts is sulfur poisoning. Studies have demonstrated that sulfur poisoning has a very negative impact on the performance of the catalysts used in industrial applications.[1,2] The identification of sulfur-tolerant catalysts remains an important and outstanding problem in catalysis.

Sulfur poisoning is a complicated phenomenon. The performance reduction induced by sulfur poisoning results from combinations of the formation of new chemical compounds on the catalyst surface, such as sulfide films; modifications in the crystal morphology; blockage of active sites by adsorbed S atoms; and changes in the electronic characteristics of the metal catalysts.[3,4] One way to improve the sulfur tolerance of metal catalysts may be to modify their electronic properties by alloying.[3,5] Therefore, understanding the interactions of S with alloy surfaces is necessary to achieve a better understanding of sulfur tolerance and to be able to identify and design sulfur tolerant catalysts. These facts have motivated many computational and experimental studies of sulfur adsorption on many different surfaces.[1,6]

Pt−Pd bimetallic catalysts have shown better performance toward hydrogenation, paraffin hydroisomerization/hydrocracking, and naphtha reforming than either of the monometallic catalysts in terms of selectivity and resistance to S poisoning and increased activity.[5] The higher sulfur tolerance of these systems was attributed to structural and electronic effects due to alloying. The reactivity of Pd surfaces is strongly modified even by small amounts of S, and Pd alloyed with Cu and Ag appears to be the most promising materials for the commercial hydrogen separation process when S poisoning is a problem.[7] It has also been reported that S−Pt bonds modify the structure of the surface Pt d-band, causing a decrease in the density of states near the Fermi level of the system and finally resulting in a reduction in the activity of the catalyst based on these electronic perturbations.[1,6] Rodriguez et al. suggested that a Pt/Sn alloy is a better option than Cu or Ag alloys for reducing the sensitivity of the Pt reforming catalyst toward S poisoning.[3] Similarly, it has been shown that SO_2 adsorption on Cu/Ag(111) surfaces differs significantly from that of pure Ag systems; the more Cu atoms there are in the alloy surface the stronger the SO_2 binding energies are.[8]

Received: January 24, 2011
Revised: February 24, 2011
Published: February 28, 2011

S poisoning of alloy systems is more difficult to understand than S poisoning of monometallic systems due to the nature of the metal−metal and sulfur−metal interactions that could lead to the occurrence of different phenomena in the alloy system from in the monometallic system. Depending on the chemical potential of S, the formation of bimetallic sulfides that exhibit very different chemical properties from those of the pure metals has been observed.[9] In some systems, S poisoning could result in surface segregation due to the stronger interaction between S and one of the metal atoms.[10,11] It is also possible to observe some alloy systems in which alloy formation causes a decrease in the affinity of S toward both metals.[3] In some systems, the presence of a specific type of atom promotes the reactivity of the other metal toward S. This effect can actually be beneficial for hydrodesulfurization catalysis.[12]

Even though it has been shown that S tolerance could be enhanced by the utilization of alloys, choosing which metals to use is still a demanding task due to the large number of combinations of metals and surface structures that could be considered. Experimental evaluation of the S tolerance requires the synthesis and characterization of a large number of alloys, which is time-consuming and expensive. These experiments need to be rationally guided to reduce the amount of work required and to accelerate the discovery of new materials.

One approach to identifying new materials uses computational tools such as density functional theory (DFT) to compute the properties of a large database of structures and then to apply screening methodologies to identify promising candidates.[13−15] At large scales (e.g., more than thousands of calculations), even DFT calculations can become prohibitively time-consuming, and simpler, more efficient models are needed. For example, Greeley showed that the adsorption energy of oxygen on a multicomponent metal site can be efficiently and reasonably approximated by a composition weighted average of the pure component adsorption energies.[15] Alternatively, one can compute a simple descriptor that is related to the catalytic property of interest through models.

One of the simple models that has been widely used to explain trends in the reactivity of transition metals using a descriptor is the d-band model.[16,17] The basic trends in the reactivity of many different transition-metal-based systems involving pure metals, surface alloys,[18,19] surfaces with strain,[20] poisons, promoters,[21] and electron deficient sites[20] are captured by the model. There are some reports in the literature showing the limitations of the d-band model in capturing the reactivity of some systems, especially those involving noble metals,[22−24] but overall, the model allows one to estimate alloy reactivity efficiently and with moderate accuracy in many cases. In a previous work in which the coverage-dependent oxygen interaction strengths with late transition metals were studied, we reported that there is a common adsorption mechanism among the late transition metals, including the noble ones, resulting in a linear correlation that relates the adsorption characteristics of different adsorbate configurations across different metal surfaces. Even though the largest deviations from the linear correlations were on the noble metal surfaces, the d-band-mediated mechanism was still sufficient to capture the majority of the adsorption energy trends, even on the noble metals.[25]

The utility of the d-band model is that very often, there is a good correlation between the d-band centers (ε_d) or the d-band widths (W_d) of a metal surface and the surface reactivity. This significantly reduces the computational expense because computing d-band properties is much cheaper than computing adsorption energies. However, this still requires a DFT calculation for each surface considered, and that can still be prohibitively expensive for large numbers of calculations. We have developed a simple, algebraic, d-band width model (the DFT parametrized solid state table) with predictive capabilities of the d-band characteristics of many different surface structures.[26,27] This model utilizes the correlation between the width of the surface d-band and the interatomic matrix element (V_{dd}) between neighboring atoms.[28] The d-band width of transition metals is directly proportional to the d-band center due to band-filling constraints. Consequently, we can very efficiently compute the d-band widths and then estimate the reactivity of alloy surfaces. The presence of adsorbates can also be taken into account by the model through the coupling matrix elements of the metal and the adsorbed atom. Thus, the model is capable of estimating the coverage dependence of the surface electronic structure, as well. The development of this simple model having predictive capabilities of d-band characteristics can be used as the basis of a screening tool for the identification of surface structures with desirable properties.

In this work, we examine the sulfur tolerance of binary combinations of 10 different late transition metal atoms (Fe, Ni, Cu, Ru, Rh, Pd, Ag, Ir, Pt, and Au) in four different surface structures (Figure 1). This requires evaluating the S tolerance of 370 surfaces. Even this is too many structures to directly evaluate using DFT. We computed the S adsorption energies and d-band widths of a subset (110) of these structures to establish a correlation between the surface electronic structure and S adsorption properties. We then used the DFT parametrized solid state table to rapidly estimate the d-band widths of all 370 structures and predicted the S adsorption energies from the DFT-derived correlation. To evaluate the stability of each structure, we utilized an atomistic thermodynamic framework that includes the effects of surface segregation, adsorption and the environmental conditions (pressure and temperature) to determine which structures were thermodynamically stable and more sulfur-tolerant than pure metals.

METHODS

In this study, we utilized the DACAPO code for all DFT calculations.[29] Both pure and alloy surface structures were modeled as slabs that were repeated periodically in a cell geometry with 10 Å of vacuum space between any two successive slabs. For each different surface structure, we utilized the fcc crystal structure with lattice constants optimized for the host metal. This is an approximation for substrates such as Fe and Ru, whose crystal structures are bcc and hexagonal, respectively. However, we anticipate that this would result in no significant effect on the final conclusions, since the estimation of the d-band characteristics depends only on the characteristic length of the metals and the interatomic distances, which do not differ very much among different crystal structures. Moreover, the metal-specific parameters have been calculated on the basis of the utilization of the fcc crystal structures for all of the late transition metals considered.[26]

Spin-polarized calculations were used where needed for slabs containing magnetic atoms. The slabs were modeled in a 2×2 unit cell consisting of 4 layers. The upper two layers were relaxed until the root-mean-squared forces were less than 0.05 eV/Å, keeping the other layers at the frozen bulk coordinates. Sulfur adsorption was performed by placing a single atom on one side of the slab corresponding to a surface coverage of 0.25 ML at its

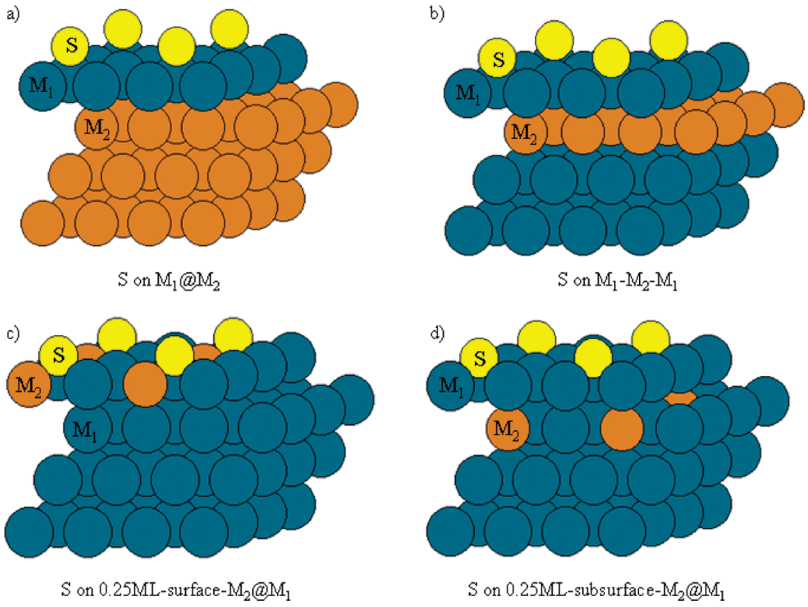

Figure 1. The binary alloy and adsorption structures considered in this work: (a) heteroepitaxial overlayer, (b) heteroepitaxial subsurface underlayer, (c) 0.25 ML surface dopant, and (d) 0.25 ML subsurface dopant. The labeling scheme used in the manuscript is indicated in each figure. The fcc adsorption site in each figure and the configurations of the considered alloys are shown.

most stable fcc adsorption site. At low coverages, this is reasonable; at higher coverages, reconstructions may occur, as well as S−S bond formation.[4,22] We are interested in identifying the onset of S poisoning; thus, the use of low coverages is appropriate. Ionic cores were described by Vanderbilt ultrasoft pseudopotentials,[30,31] and the one-electron valence eigenstates were expanded in a plane wave basis set with a cutoff energy of 340 eV. The exchange correlation functional used was the generalized gradient approximation (GGA) due to Perdew−Wang (PW91).[32] Brillouin-zone integrations were performed using a 6 × 6 × 1 Monkhorst-Pack grid for the 2 × 2 surface unit cell. In our experience, these calculation parameters lead to convergence in the S adsorption energies of less than 50 meV/adsorbate. The atom-projected d-bands were calculated by projecting the computed wave functions onto atomic orbitals localized on each atom. The d-band width is calculated as the square root of the second moment of the d-band with respect to the Fermi level as $W_d = (\int \rho E^2\, dE / \int \rho\, dE)^{1/2}$.

For each heteroepitaxial overlayer alloy structure, we utilized three substrate layers and one surface layer. The lattice constants of the bimetallic structures were dictated by the lattice constant of the substrate (host) atom. In total, we considered binary combinations of 10 different late transition metal atoms (Fe, Ni, Cu, Ru, Rh, Pd, Ag, Ir, Pt, and Au) in four different surface structures (Figure 1).

The stability of alloy systems can be evaluated by comparing the surface free energies to reference systems. The most stable surface structure is the one that minimizes the surface free energy, γ, which is a function of temperature, pressure, and composition. We express the surface free energy as[33]

$$\gamma(T, p, N_{slab}, x_i, N_s) = \gamma_{host} + \frac{E_{seg}}{A_{surf}} + \frac{N_S E_{ads}(0\ K)}{A_{surf}} - \frac{N_S \Delta\mu_S}{A_{surf}} \quad (1)$$

In the above surface free energy expression, γ_{host} is the surface free energy for the clean surface of the host metal. E_{seg} corresponds to the segregation of an impurity atom from the bulk to the surface.[34] A negative value for E_{seg} indicates favorable segregation to the surface. We have assumed in this work that the segregation energy contribution is not alloy-concentration-dependent. We define the S adsorption energy at 0 K (in the approximation where $\Delta G \approx \Delta E$) as

$$E_{ads}(0\ K) = \frac{1}{N_S}\left[E_{slab}(N_{slab}, N_S) - E_{slab}^{clean}(N_{slab}) - N_S E_S\right] \quad (2)$$

Negative S adsorption energies are exothermic.

The S chemical potential, μ_S, is expressed in terms of the difference in chemical potentials of gas phase H_2S and H_2. For S adsorption, if the S chemical potential becomes equal to or greater than that of bulk S (S-rich conditions), then S will begin to condense on the surface and form the bulk S phase (in addition to possibly forming bulk metal sulfides), leading to a total deactivation of the surface. There is no lower limit for the S chemical potential; a chemical potential of $-\infty$ corresponds to a gas-phase environment with no sulfur in it. We define $\Delta\mu_S$ as $\mu_S - E_S^{bulk}$.[4] We used the α phase of S for E_S^{bulk} and shifted the limits to have the S-rich chemical potential at zero so that the range for the S chemical potential is expressed from $-\infty$ to zero. The surface energy equation shows that at a fixed S chemical potential, more stable surface structures (with lower surface energies) can be achieved by an exothermic S adsorption, by energetically favorable surface segregation, or by some favorable combination of adsorption and segregation. For example, an unfavorable segregation energy can be compensated by a very favorable adsorption energy.

The surface energy equation can be used to compute the chemical potential of S that will result in sulfur poisoning. For example, the onset of S adsorption occurs when the surface energy of a surface with sulfur on it is equal to the surface energy of the clean surface. Since the surface energy is a function of the sulfur chemical potential, one can compute the chemical potential which determines the onset of S adsorption; the onset

dx.doi.org/10.1021/cs200039t |ACS Catal. 2011, 1, 399–407

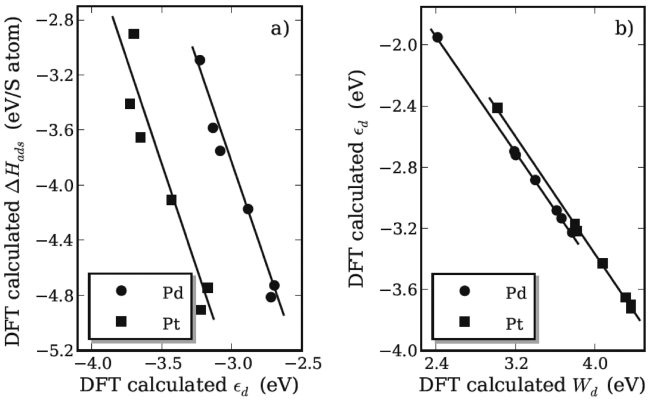

Figure 2. (a) Sulfur adsorption energies at six different coverages from 0.25 to 1 ML on Pd and Pt metal (111) facets as a function of the d-band center. (b) d-Band centers of the configurations in panel a as a function of the d-band widths. The clean surface d-band properties are also included, which correspond to the ones having the highest d-band center in average energy and the narrowest d-band width for both of the Pd and Pt metallic systems.

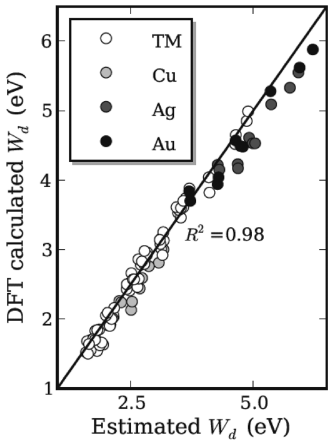

Figure 3. Parity plot of d-band widths for clean heteroepitaxial overlayer combinations of late transition metals. The legend corresponds to the composition of the overlayer (Cu, Ag, and Au; TM stands for the other transition metals) on top of different types of host atoms.

chemical potential is simply $\Delta\mu_S = E_{ads}(0\ K)$. In this context, a more sulfur-tolerant surface will require a higher chemical potential of sulfur before poisoning occurs.

RESULTS AND DISCUSSION

d-Band Characteristics and Adsorption Properties. Adsorption energies are often correlated with the surface d-band center (ε_d). We observed near linear correlations between the calculated sulfur adsorption energies at six different coverages (2 × 2−0.25 ML, $\sqrt{3} \times \sqrt{3}$R30° − 1/3 ML, 2 × 1 − 0.5 ML, $\sqrt{3} \times \sqrt{3}$R30° − 2/3 ML, 2 × 2 − 0.75 ML, and 1 × 1 − 1 ML) on Pd and Pt (111) surfaces and the surface d-band center (Figure 2a). The surface d-band center is linearly correlated with the surface d-band width based on the rectangular d-band model (Figure 2b) for each of the six coverages and the clean surface.[18,35] These results show that one can estimate changes in the adsorption energy from changes in the surface d-band width.

Moreover, it has been well established that the estimation of the adsorption properties could be achieved from clean surface properties, particularly from the surface d-band center. For instance, oxygen binding energies over transition metal alloys have been estimated by incorporating the changes in ligand, strain effects, and chemical composition into the surface d-band center.[15] Since the shifts in d-band characteristics and adsorption properties are correlated, the reactivities of alloy surfaces toward S can be estimated if the d-band characteristics of the surface structures are known. Our previous studies[26,27] demonstrated that the surface d-band width can readily be estimated using the DFT parametrized solid state table.

Estimating d-Band widths. Interatomic matrix elements describe the bonding interactions between the d states of atoms in terms of their corresponding characteristic orbital sizes (r_d) and the spacing between the metals (d_{ij}). The matrix elements can be expressed as $V_i \approx \Sigma_j ((r_d^{(i)} r_d^{(j)})^{3/2})/d_{ij}^{5}$.[28] On the basis of the tight binding theory, these interatomic matrix elements are correlated with d-band widths. We developed a model that accounts for the sharpening/broadening of the d-band due to the interaction of all neighboring atoms through their characteristic orbital sizes and their corresponding atomic separation. For surfaces, we account for a facet-specific redistribution of electron density near the surface due to the loss of bulk symmetry. These contributions lead W_d to take the following form,

$$W_{d,i} = W_{o,i} + \sum_j \frac{\left(r_d^{(i)} r_d^{(j)}\right)^{3/2}}{d_{ij}^{5}} + \beta \qquad (3)$$

where $W_{o,i}$ is the nonzero band width of an atom i at infinite separation, which is an artifact of the d-band width being defined as the square root of the second moment of the d-band about the Fermi level. β is a facet-specific constant that accounts for the effects of surface relaxation on the d-band width. The details of the model and the values for each parameter (the solid state table) can be found elsewhere.[26,27] The model works for monometallic and bimetallic surfaces in a variety of surface structures (e.g., (111), (100), (110) surfaces, etc.).

We considered different combinations of heteroepitaxial overlayers and estimated their corresponding surface d-band widths by utilizing the solid state table. The agreement between the estimated and the DFT calculated surface d-band widths of 110 heteroepitaxial overlayer combinations is excellent (Figure 3). The mean absolute error in the estimation is <4.5%. The outliers generally correspond to the binary systems involving Ag or Au as the overlayer. This can be attributed to the large relaxations caused by the large differences between the lattice constants of these atoms and the other late transitions metals. In the estimation of the d-band widths, the unrelaxed distances between the atoms are determined by the lattice constant of the host atoms. This simplification works well for systems with similar lattice constants (e.g. Ag/Au or Pd/Pt alloys) because relaxation effects are small. The simplification begins to fail for systems with very different lattice constants; for example, Cu/Au alloys.

Estimation of Sulfur Adsorption Properties. We computed the adsorption energies of S on the sites shown in Figure 1 for the heteroepitaxial overlayer structures. The correlations between the DFT-calculated S adsorption energies and the d-band widths for the 110 heteroepitaxial overlayer combinations are shown in Figure 4a. Each structure has its own correlation. The correlations for Au- and Ag-containing structures were very poor. The poor correlation is not due to poor estimates of the d-band widths

dx.doi.org/10.1021/cs200039t |ACS Catal. 2011, 1, 399–407

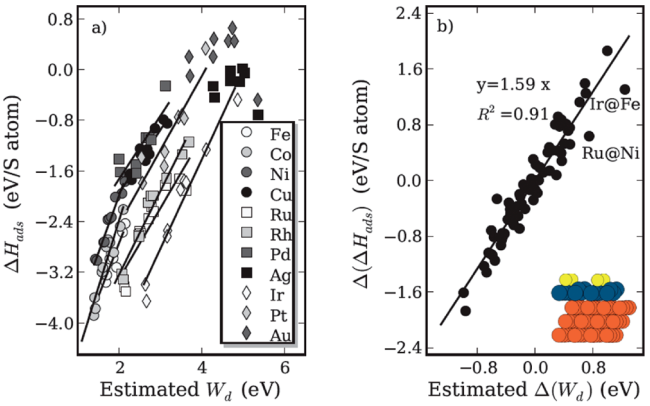

Figure 4. (a) Correlation between DFT calculated S adsorption energies and estimated d-band widths for different heteroepitaxial overlayer combinations. The legend identifies the composition of the overlayer. (b) Correlation between shifts in DFT calculated S adsorption energies and shifts in estimated d-band widths. The shifts are calculated with respect to the pure metallic systems. The inset figure shows a typical reconstruction observed on the labeled Ir@Fe and Ru@Ni surface structures.

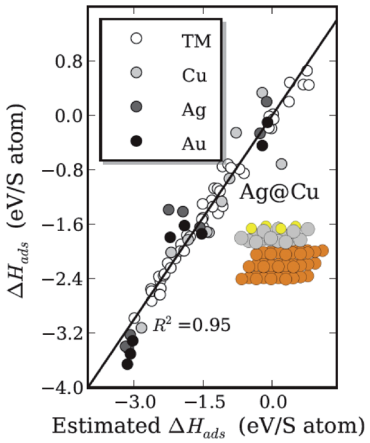

Figure 5. Parity plot of S adsorption energies over heteroepitaxial overlayer combinations. The legend corresponds to the same host (Cu, Ag, and Au; TM stands for the other transition metals) with different types of overlayer atoms. The inset figure shows the reconstructions observed in Ag@Cu alloy system.

for Ag- and Au-based systems (Figure 3). In these systems, the discrepancy can be attributed to the completely filled d-band states of these noble metals, resulting in additional types of interactions with sulfur (e.g., Pauli repulsion or interadsorbate bonding) that are not accounted for in the simple d-band model or in our tight-binding model.[26,27] For these outliers, the d-band characteristics do not fully capture the reactivity of the surfaces toward S. Excluding the Ag- and Au-based systems, the system-specific correlations between S adsorption energies and surface d-band widths collapse to a $y = 1.59x$ line if shifts in adsorption characteristics $\Delta(\Delta H_{ads})$ and shifts in the d-band widths $\Delta(W_d)$ with reference to that of their values in pure metallic systems are considered (Figure 4b). The statistical analysis of the fitted line returns an uncertainty of ± 0.045 in the slope, yielding it to take values in the range of 1.54−1.63. The propagation of this error as well as the one in the estimated d-band widths will be discussed further throughout the manuscript.

The most outlying data correspond to structures with reconstructions. Some examples of reconstructions observed in this work are Ir@Fe and Ru@Ni heteroepitaxial overlayer combinations in which the surface Ir (Ru) atoms not bonded directly to the S adatom show rumpling (inset in Figure 4b). For these systems, the clean surface d-band properties are insufficient to capture the surface reactivity due to the structure changes and corresponding changes in bonding that occur. This is one of the main limitations of the solid state table; we estimate the d-band widths of the surface atoms from unrelaxed bond lengths determined by the host. If significant relaxation or reconstruction occurs, the estimated d-band widths deviate more significantly from the DFT values, and the bonding contributions to the adsorption deviate from the simple d-band model more significantly. Better agreement with the DFT results can be obtained using the actual relaxed metal distances, but this requires that one know the geometry in advance. Even with these problematic systems, the good linearity of the correlation between $\Delta(\Delta H_{ads})$ and $\Delta(W_d)$ suggests that we can utilize the linear relationships associated with the estimated d-band widths to predict S adsorption energies over the investigated transition metal alloy structures. We show the agreement between the DFT calculated and estimated adsorption energies over the (111) facets of the heteroepitaxial overlayer alloy surfaces in Figure 5. The error analysis designates that the model predicts 86% of its database within ±15%, and 92% of its database within ±20% of the DFT value.

The outliers correspond to the binary structures involving Cu, Ag, or Au metals. The inset figure demonstrates the reconstructions observed in a Ag@Cu system in which the surface Ag atoms show rumpling (inset in Figure 5). Excluding the systems in which d-band model cannot fully capture the reactivity of the systems, the mean absolute error in estimating S adsorption properties is <6%, which demonstrates the feasibility of using the simple algebraic solid state table model to estimate reactivity.

The approach outlined here could be more broadly useful than simply predicting sulfur adsorption energies. There exist scaling relationships in the literature that relate the adsorption energies of CH, CH_2, and CH_3 to the adsorption energy of C, of NH and NH_2 to the adsorption energy of N, of OH to the adsorption energy of O, and of SH to the adsorption energy of S.[36,37] Thus, provided correlations exist between the electronic structure properties that are easy to compute and reactivity properties that are desired, it may be possible to construct sophisticated screening methods to identify materials with desired reactive properties.

The determination of S-tolerant surface structures cannot be achieved only by looking at the S adsorption energy. Reactive environmental conditions and surface segregation energies play an important role in determining the stability of the investigated systems. For example, it is easy to put a Au monolayer on Cu to make it more S-tolerant because S bonds more weakly to Au. However, S bonds more strongly to Cu, and an adsorbate-induced segregation of Cu is possible, depending on the environmental conditions. Furthermore, the Au monolayer would be under substantial compressive strain and likely would not be stable. Thus, the Au monolayer is not a stable, S-tolerant structure. An atomistic thermodynamic approach is needed to account for the effects of segregation and environment. We do not consider the effect of strain on stability in this work.

Atomistic Thermodynamics Approach to Sulfur-Tolerant Surface Structures. We used an atomistic thermodynamic formalism to compute the sulfur tolerance of each structure in

dx.doi.org/10.1021/cs200039t |*ACS Catal.* 2011, 1, 399–407

Table 1. S Chemical Potentials Where the Corresponding Binary Alloy Structure Starts To Become S-Poisoned Due to Adsorption[a]

Metal		
Metal	M_1@M_2	M_1-M_2-M_1
	0.25ML surface M_2@M_1	0.25ML subsurface M_2@M_1

Substrate / Dopant atoms (M_2)		Surface metal atom (M_1)																			
		Fe		Ni		Cu		Ru		Rh		Pd		Ag		Ir		Pt		Au	
Substrate / Dopant atoms (M_2)	Fe	**-2.43**		-1.84	-1.99	-0.46	-1.06	-0.91	-2.75	-0.53	-2.46	0.53	-1.95	2.36	-0.60	0.20	-2.58	1.34	-2.26	3.88	-0.75
				-1.93	-1.97	-1.41	-0.97	-2.77	-2.49	-2.42	-2.15	-1.82	-1.65	-1.71	-0.38	-2.62	-2.05	-2.18	-1.77	-1.23	-0.32
	Ni	-	-2.39	**-1.95**		-0.60	-1.03	-	-2.72	-	-2.43	0.24	-1.92	2.08	-0.57	-	-2.53	-	-2.22	3.45	-0.72
		-	-2.42			-1.43	-0.96	-	-2.47	-	-2.14	-1.84	-1.64	-1.74	-0.37	-	-2.03	-	-1.76	-1.26	-0.31
	Cu	-	-2.29	-	-1.85	**-0.93**		-	-2.62	-	-2.32	-0.38	-1.82	1.47	-0.50	-	-2.41	-	-1.84	2.50	-0.64
		-	-2.38	-	-1.92			-	-2.44	-	-2.10	-1.34	-1.61	-1.27	-0.34	-	-1.99	-	-1.63	-0.76	-0.28
	Ru	-3.03	-2.02	-2.49	-1.58	-1.30	-0.67	**-2.35**		-2.10	-2.04	-1.12	-1.58	0.76	-0.31	-2.00	-2.10	-0.98	-1.84	1.37	-0.41
		-1.99	-2.29	-1.50	-1.83	-1.00	-0.84			-1.97	-2.01	-1.43	-1.53	-1.42	-0.28	-2.10	-1.89	-1.74	-1.63	-0.87	-0.20
	Rh	-	-1.97	-2.43	-1.54	-1.22	-0.62	-	-2.31	**-1.99**		-1.01	-1.53	0.87	-0.27	-	-2.04	-0.84	-1.79	1.53	-0.37
		-	-2.28	-1.53	-1.81	-1.02	-0.83	-	-2.34			-1.46	-1.51	-1.46	-0.27	-	-1.87	-1.76	-1.61	-0.91	-0.19
	Pd	-	-1.94	-	-1.50	-	-0.59	-	-2.28	-	-1.96	**-1.50**		0.39	-0.25	-	-2.00	-	-1.76	0.82	-0.34
		-	-2.27	-	-1.80	-	-0.82	-	-2.33	-	-1.98			-1.51	-0.26	-	-1.86	-	-1.60	-0.95	-0.18
	Ag	-	-1.96	-	-1.52	-	-0.61	-	-2.30	-	-1.77	-	-1.52	**-0.26**		-	-2.03	-	-1.78	-0.14	-0.36
		-	-2.27	-	-1.81	-	-0.82	-	-2.33	-	-1.92	-	-1.51			-	-1.86	-	-1.61	0.29	-0.19
	Ir	-	-1.75	-2.36	-1.32	-1.15	-0.41	-	-2.10	-1.91	-1.77	-0.93	-1.33	0.95	-0.12	**-1.78**		-0.76	-1.57	1.60	-0.18
		-	-2.20	-1.24	-1.74	-0.75	-0.76	-	-2.27	-1.70	-1.92	-1.20	-1.45	-1.25	-0.21			-1.47	-1.54	-0.66	-0.13
	Pt	-	-1.71	-	-1.28	-	-0.37	-	-2.06	-	-1.73	-1.50	-1.30	0.40	-0.09	-	-1.74	**-1.53**		0.79	-0.15
		-	-2.19	-	-1.73	-	-0.74	-	-2.26	-	-1.90	-1.26	-1.44	-1.32	-0.20	-	-1.77			-0.72	-0.12
	Au	-	-1.65	-	-1.23	-	-0.32	-	-2.00	-	-1.67	-	-1.25	-0.21	-0.05	-	-1.67	-	-1.47	**-0.10**	
		-	-2.17	-	-1.71	-	-0.73	-	-2.24	-	-1.89	-	-1.42	-0.70	-0.19	-	-1.75	-	-1.51		

[a] The values in bold correspond the S chemical potential where monometallic surfaces start to get S-poisoned. The red cells designate alloys with less S tolerance than the parent metal, whereas the gray cells correspond to the structures with enhanced S tolerance. Empty cells with a dash in them do not have thermodynamically favorable segregation energies. The columns represent the metals at the surface; whereas the rows designate the substrate or the host metals.

the database of 370 structures considered. This S tolerance is determined as the S chemical potential beyond which the surface structure becomes S-poisoned due to its lower surface free energy than that of the clean structure. The transition between the stabilities of the clean and S-poisoned structures occurs when the surface free energies of the clean and the S-poisoned structures become equal. The results are tabulated in Table 1 for all the structures that are determined to be thermodynamically stable with respect to segregation. The values given in bold designate the S chemical potential where the monometallic surface in its normal structure starts to become S-poisoned; that is, the onset of S adsorption at 0.25 ML. The empty entries correspond to the structures with unfavorable segregation properties. The red entries indicate systems with less S tolerance; whereas the gray ones designate the surface structures with enhanced S tolerance. The darker the gray, the more S-tolerant the structures are. The uncolored white cells correspond to the structures with the same S tolerant characteristics as the monometallic surfaces.

In general, S tolerance of the alloys increases when the metals are alloyed with metals having a smaller lattice parameter. This is due to an increase in the overlap of the d orbitals of the corresponding metal atoms. The increased overlap results in a broadening of the d-band and in a lowering of d-band centers in energy, with a corresponding reduction in the S adsorption energy. The same phenomenon of enhanced S tolerance also applies for $M_1-M_2-M_1$ type alloys when the lattice constant of M_2 is greater than M_1. The presence of the type of metal atoms with larger characteristic length causes an increase in the overlap of the d orbitals that would results in the broadening of d-band widths. This leads to weaker S adsorption properties of the surface structures. To observe more highly S-tolerant structures with 0.25 ML surface (subsurface) M_2@M_1 alloys, the dopant should have a much larger lattice parameter than the substrate atoms. This can be attributed to the low coverage of dopant in the structures; only the metals with very large lattice parameters could show the effect in terms of increased overlap and could result in weaker S adsorption properties.

The effect of error propagation on the S tolerance characteristics have been calculated by considering the error in the estimated d-band widths and the uncertainty in the fit of the shifts in adsorption characteristics $\Delta(\Delta H_{ads})$ and shifts in d-band widths $\Delta(W_d)$. This leads to the estimation of different S adsorption energies for the same surface structure. The mean of the standard deviation over all surface structures for the predicted adsorption energies was found to be <0.018 eV. The range of the estimated S adsorption energies leads to a range in the S chemical potential onsets of ±3%.

dx.doi.org/10.1021/cs200039t |*ACS Catal.* 2011, 1, 399–407

For systems in which noble metals are involved, some additional care in interpreting the results may be required. We reported some deviations in the estimated S characteristics of these noble-metal-based systems (Figure 5). The interactions between adsorbates and these metals involve an increased contribution from Pauli repulsion that works in the direction opposite the antibonding mechanism. The general trends in the modifications of the reactivities of these systems are captured; for example, adsorption of these systems is weaker, as expected. In addition, d-band-mediated mechanisms have been utilized to provide explanations for the interactions between oxygen and noble metals.[25] This is due to the fact that explanations of the modifications in the adsorptions characteristic of the metallic systems have been provided on the basis of the coupling of the metal d orbitals, which governs the ultimate principles of underlying physics. However, because of the possibility of large relaxations in systems containing noble metals and other smaller atoms, one must keep in mind that the estimations of the ideal geometry may not reflect the reactivity of relaxed geometries. The results should, nevertheless, be utilized as part of the motivation for deeper investigations with more accurate models.

Application to S-Tolerance for a Specific Metal. S poisoning is a great issue for Cu-based systems. The presence of even small amounts of S in the feed streams can cause the deactivation of the catalyst because of the formation of a strong bond between the adsorbate and the surface metal atoms.[38−40] To illustrate how our approach can be used to identify sulfur-tolerant catalysts, we apply the method to Cu-based systems having Cu as their surface atoms (M_1). Cu is known to be the best pure metal for the low temperature water gas shift reaction used in hydrogen generation from fossil fuels.[41] Under normal operating conditions, in the water gas shift reaction, there are S impurities which can adsorb onto Cu surfaces and block the active sites of the catalyst for the desired reaction and can result in catalyst deactivation.[1,2,7] The estimated S adsorption energies on the Cu-based alloy structures and the results are shown in Figure 6.

Weaker S adsorption energies are obtained when Cu is alloyed with Fe or Ni to form $M_1@M_2$ type of alloys; with 4d and 5d metals to form $M_1-M_2-M_1$; or with Ag, Ir, Pt, or Au to form 0.25 ML surface and subsurface $M_2@M_1$ alloys. For Cu@Fe and Cu@Ni systems, the lattice constants are dictated by Fe and Ni substrates, which are smaller than the lattice constant of monometallic Cu. Smaller lattice constants result in compressive strain, leading to an increase in the overlap of the d orbitals of neighboring metal atoms. The increased overlap results in a broadening of the d-band. The broader bands have lower surface d-band centers in energy and, consequently, interact more weakly with adsorbates, leading to weaker S adsorption properties. When Cu is alloyed with 4d or 5d metals to form $M_1-M_2-M_1$ and 0.25 ML subsurface $M_2@M_1$ types of alloys, the increase in the overlap of the d orbitals due to the larger characteristic orbital sizes of these 4d and 5d metals also results in the broadening of the d-band width and lowering of the surface d-band in energy. The same phenomenon holds for 0.25 ML surface $M_2@M_1$ alloys with large characteristic orbital sizes of the dopants. Since the dopant is at 0.25 ML, only the metals with a very large r_d could show the effect in terms of increased overlap and, thus, could result in weaker S adsorption properties.

To illustrate how S tolerance is enhanced, we have calculated the surface free energies of clean (horizontal lines) and S-poisoned (corresponding lines with negative slopes) binary alloy combinations for selected Cu-based systems. Below, we have

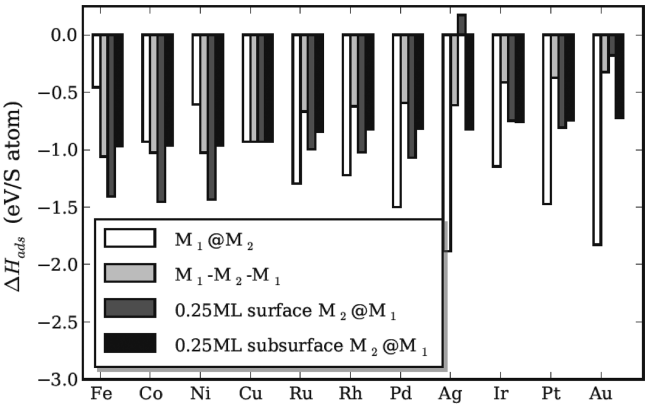

Figure 6. Estimated S adsorption energies over Cu-based catalyst with different binary alloy structures: heteroepitaxial overlayer, heteroepitaxial subsurface underlayer, 0.25 ML surface dopant, and 0.25 ML subsurface dopant. The *x* axis designates the second metal in the binary alloys. For the pure metallic case, the estimated S adsorption energies are the same for each different surface structure considered.

considered only two of the stable structures for the purpose of illustrating sulfur tolerance: one with less and one with more S tolerant characteristics than a monometallic Cu system (Figure 7).

The S-poisoned monometallic Cu system starts to form at a S chemical potential of −0.93 eV (the intersection of the solid and dashed lines for Cu). The partial pressures of gas phase H_2S to H_2 at different temperatures that correspond to this S chemical potential could be looked up in the Janaf Thermochemical Tables,[42] similar to our previous work.[4] For a surface to have a higher S tolerance, the initial S adsorption needs to occur at a chemical potential more positive than −0.93 eV. For example, enhanced S tolerance can be obtained when Cu is alloyed with Ir to form $M_1-M_2-M_1$ type alloys. In contrast, Cu@Ru shows less S tolerance; S-poisoned surfaces become thermodynamically more favorable than a clean surface at a S chemical potential of −1.30 eV, which is lower than the value of −0.93 eV for a monometallic Cu system. In other words, the Cu@Ru system is poisoned at a lower concentration of sulfur in the environment than a pure Cu surface. This is due to the larger lattice constant of Ru that leads to tensile strain in the Cu overlayer, causing a narrower d-band width and higher d-band center with increased activity toward S poisoning.

Our findings suggest that Pd alloyed with Cu (Pd@Cu) shows enhanced S tolerance characteristics when compared with pure Pd metallic system. Moreover, an experimentally more realistic case, a 0.25 ML surface Cu@Pd bimetallic structure, also results in resistive S characteristics. This Pd−Cu alloy combination has been used as the catalyst membrane in hydrogen separation and is known to be sulfur-tolerant. Iyoha and his co-workers[43] also reported sulfur-tolerant Pd−Au alloy membranes for hydrogen separation processes. The authors suggest that a Pd−Au system demonstrates negligible chemical interaction between the H_2S feed and the alloy membranes. They attributed the lack of the sulfidization of the Pd−Au alloys to the possible surface enrichment of the alloy with Au as a result of Au segregation at the membrane surface. In agreement with these experimental findings, our simple approach also suggests enhanced S tolerance of Au@Pd over the pure metallic Pd system. Moreover, our simple model combined with atomistic thermodynamic approach captures the enhanced S characteristics of Pt-based systems

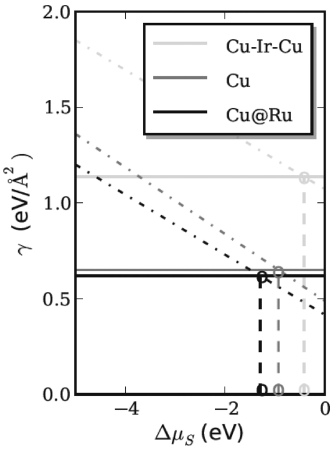

Figure 7. Surface free energies of Cu-based catalyst surface structures as a function of S chemical potential. Horizontal lines designate the surface free energies of the clean structures, whereas their corresponding lines with negative slopes refer to the S-poisoned cases of the same structures. The "o" corresponds to S chemical potentials at which S-poisoned structures would become thermodynamically more favorable than their corresponding clean surfaces. Vertical dashed lines are to guide the eye.

when alloyed with Au to form 0.25 ML subsurface Au@Pt and Pt−Au−Pt surface structures.[6] The reason for S resistivity is attributed to the increase in the overlap of d-orbitals due to the presence of Au atoms in the structures. Conversely, S interacts more strongly with Cu atoms in Cu−Ag alloys than that of pure Ag systems as a result of the smaller characteristic radius of the Cu d orbitals, which results in a reduced orbital overlap of the d states compared with pure Ag. This causes a narrowing of the d-band width and higher d-band center in energy. Finally, with increased interaction with S, similar results have been reported previously.[8]

Our findings suggest that Rh-based systems become more S tolerant when alloyed with Au, which is in good agreement with the study by Rodriguez et al.[44] The demonstration of the predictive capability of our proposed approach is not limited to only the above-mentioned examples. In this work, Pd@Rh, 0.25 ML subsurface Rh@Pd and Rh−Pd−Rh, 0.25 ML surface Pd@Rh show better S characteristics than that of their pure metallic systems. This may be one reason for the use of a Pd/Rh-based system for the automotive exhaust catalyst in catalytic converters; the bimetallic Pd−Rh catalyst may have a higher sulfur tolerance than pure Pt.

This approach presented here is a coarse-grained way to screen a very large number of alloy structures for S tolerance. Pools of potentially S-tolerant compositions must be chosen judiciously because several simplifications are made in the process to make the computations very fast. For example, the segregation energies are approximated as the impurity segregation energies from pure bulk metals. In real alloy systems, the segregation energy depends on the bulk structure and composition[32] as well as the surface and temperature. As promising candidates are identified, one would naturally choose to investigate them more deeply with more accurate models. The approach presented here could be part of the motivation for deeper investigations of promising candidates.

CONCLUSIONS

We utilized a DFT parametrized solid state table to estimate the d-band characteristics of transition metal-based binary alloys and their corresponding reactivities toward S poisoning. The results were validated on a subset of 110 DFT calculations. We considered a total of 370 different surface alloy configurations and assessed their sulfur tolerance using an atomistic thermodynamic framework. It is in general possible to increase or decrease the S tolerance of a metal by alloying and to identify alloys that are likely to be stable under reaction conditions. The approach presented here should be viewed as a first step in identifying sulfur-tolerant alloys when one seeks to focus from a very large number of catalyst composition possibilities to a smaller, reasonable number of possibilities.

ASSOCIATED CONTENT

Supporting Information. A pdf containing a summary of the atomic geometry and calculation parameters for each calculation in this work is available. This material is available free of charge via the Internet at http://pubs.acs.org.

AUTHOR INFORMATION

Corresponding Author
*E-mail: jkitchin@andrew.cmu.edu.

ACKNOWLEDGMENT

J.R.K. gratefully acknowledges support of this work in part by the Office of Basic Energy Science of the U.S. Department of Energy (Grant No. DOE-BES DEFG0207ER15919).

REFERENCES

(1) Bartholomew, C. H.; Agrawal, P. K.; Katzer, J. R. *Adv. Catal.* **1982**, *31*, 135.
(2) Rodriguez, J. A.; Hrbek, J. *Acc. Chem. Res.* **1999**, *32*, 719.
(3) Rodriguez, J. A.; Hrbek, J.; Kuhn, M.; Jirsak, T.; Chaturvedi, S.; Maiti, A. *J. Chem. Phys.* **2000**, *113*, 11284.
(4) İnoğlu, N.; Kitchin, J. R. *J. Catal.* **2009**, *261*, 188.
(5) Jiang, H.; Yang, H.; Hawkins, R.; Ring, Z. *Catal. Today* **2007**, *125*, 282.
(6) Rodriguez, J. A.; Kuhn, M.; Hrbek, J. *Chem. Phys. Lett.* **1996**, *251*, 13.
(7) Alfonso, D. R.; Cugini, A. V.; Sholl, D. S. *Surf. Sci.* **2003**, *546*, 12.
(8) Zhao, X. Y.; Liu, P.; Hrbek, J.; Rodriguez, J. A.; Perez, M. *Surf. Sci.* **2005**, *592*, 25.
(9) Rodriguez, J. A.; Kuhn, M. *J. Phys. Chem.* **1995**, *99*, 9567.
(10) Kuhn, M.; Rodriguez, J. A. *J. Phys. Chem.* **1994**, *98*, 12059.
(11) Kuhn, M.; Rodriguez, J. A. *Chem. Phys. Lett.* **1994**, *231*, 199.
(12) Kuhn, M.; Rodriguez, J. A. *Surf. Sci.* **1996**, *355*, 85.
(13) Greeley, J.; Nørskov, J. K. *Surf. Sci.* **2007**, *601*, 1590.
(14) Greeley, J.; Jaramillo, T. F.; Bonde, J.; Chorkendorff, I. B.; Nørskov, J. K. *Nat. Mater.* **2006**, *5*, 909.
(15) Greeley, J.; Nørskov, J. K. *Surf. Sci.* **2005**, *592*, 104.
(16) Hammer, B.; Nørskov, J. K. *Nature* **1995**, *376*, 238.
(17) Hammer, B.; Nørskov, J. K. *Surf. Sci.* **1995**, *343*, 211.
(18) Kitchin, J. R.; Nørskov, J. K.; Barteau, M. A.; Chen, J. G. *J. Chem. Phys.* **2004**, *120*, 10240.
(19) Greeley, J.; Mavrikakis, M. *J. Phys. Chem. B* **2005**, *109*, 3460.
(20) Mavrikakis, M.; Hammer, B.; Nørskov, J. K. *Phys. Rev. Lett.* **1998**, *81*, 2819.
(21) Mortensen, J. J.; Hammer, B.; Nørskov, J. K. *Phys. Rev. Lett.* **1998**, *80*, 4333.
(22) İnoğlu, N.; Kitchin, J. R. *Mol. Simul.* **2009**, *35*, 936.
(23) Hyman, M. P.; Loveless, B. T.; Medlin, J. W. *Surf. Sci.* **2007**, *601*, 5382.
(24) Xin, H.; Linic, S. *J. Chem. Phys.* **2010**, *132*, 221101.

(25) Miller, S. D.; İnoğlu, N.; Kitchin, J. R. *J. Chem. Phys.* **2011** in press.
(26) İnoğlu, N.; Kitchin, J. R. *Phys. Rev. B* **2010**, *82*, 045414.
(27) İnoğlu, N.; Kitchin, J. R. *Mol. Simul.* **2010**, *36*, 633.
(28) Harrison, W. A. *Electronic Structure and the Properties of Solids*; Dover Publication, Inc.: New York, 1989.
(29) DACAPO; https://wiki.fysik.dtu.dk/dacapo.
(30) Vanderbilt, D. *Phys. Rev. B* **1993**, *41*, 7892.
(31) Laasonen, K.; Pasquarello, A.; Car, R.; Lee, C.; Vanderbilt, D. *Phys. Rev. B* **1993**, *47*, 10142.
(32) Perdew, J. P.; Wang, Y. *Phys. Rev. B* **1992**, *45*, 13244.
(33) Kitchin, J. R.; Reuter, K.; Scheffler, M. *Phys. Rev. B* **2008**, *77*, 075437.
(34) Christensen, A.; Ruban, A. V.; Stoltze, P.; Jacobsen, K. W.; Skriver, H. L.; Nørskov, J. K.; Besenbacher, F. *Phys. Rev. B* **1997**, *56*, 5822.
(35) Kitchin, J. R.; Nørskov, J. K.; Barteau, M. A.; Chen, J. G. *Phys. Rev. Lett.* **2004**, *93*, 156801.
(36) Abild-Pedersen, F.; Greeley, J.; Studt, F.; Rossmeisl, J.; Munter, T. R.; Moses, P. G.; Skulason, E.; Bligaard, T.; Nørskov, J. K. *Phys. Rev. Lett.* **2007**, *99*, 016105.
(37) Jones, G.; Bligaard, T.; Abild-Pedersen, F.; Nørskov, J. K. *J. Phys. Condens. Matter* **2008**, *20*, 064239.
(38) Rodriguez, J. A.; Chaturvedi, S.; Jirsak, T. *Chem. Phys. Lett.* **1998**, *296*, 421.
(39) Gravil, P. A.; Toulhoat, H. *Surf. Sci.* **1999**, *430*, 176.
(40) Feibelman, P. J.; Hamann, D. R. *Surf. Sci.* **1985**, *149*, 48.
(41) Schumacher, N.; Boisen, A.; Dahl, S.; Kandoi, S.; Grabow, L. C.; Dumesic, J. A.; Mavrikakis, M.; Chorkendorff, I. *J. Catal.* **2005**, *229*, 265.
(42) Stull, D. R.; Prophet, H. *Janaf Thermochemical Tables*, 2nd ed.; National Standards Reference Data Series, National Bureau of Standards: Washington D.C., 1971.
(43) Iyoha, O.; Enick, R.; Killmeyer, R.; Morreale, B. *J. Membr. Sci.* **2007**, *305*, 77.
(44) Rodriguez, J. A.; Kuhn, M.; Hrbek, J. *J. Phys. Chem.* **1996**, *100*, 3799.